Thermoelastic Properties of Plain Weave Composites for Multilayer Circuit Board Applications

N. R. Sottos

J. M. Ockers

M. Swindeman

University of Illinois at Urbana-Champaign,
Department of Theoretical
and Applied Mechanics,
216 Talbot Laboratory,
104 South Wright Street,
Urbana, IL 61801

The thermoelastic properties of woven glass/epoxy substrates for multilayer circuit board applications were investigated and the influence of fabric geometry assessed. The woven fabric geometry of several commercially pressed boards was carefully characterized using optical microscopy. The elastic moduli and Poisson's ratios were then measured in uniaxial tension, while the CTEs of the boards were measured using thermal mechanical analysis (TMA) at temperatures above and below the glass transition. Experimental data were compared to predictions from two new analytical models. One of the models, which does not use classical lamination theory, results in a significant improvement for the prediction of Poisson's ratio and CTEs. Finally, a parametric study was performed to demonstrate the effect of fiber crimp on the properties of the fabric.

Introduction

Woven glass/epoxy composites are used extensively as substrate materials for multilayer printed circuit boards. The boards are fabricated by consolidating layers of copper and glass/epoxy prepreg in a press under a prescribed temperature and pressure cycle. Significant thermal residual stresses develop during the manufacturing and post manufacturing processes which cause in-elastic deformation in the boards. Residual stresses are caused by differential thermal expansion of the plies and curing shrinkage of the resin. Post-manufacturing processes such as solder masking, solder reflow, and wave soldering also generate residual stresses and strains. These stresses may be large enough to cause plastic deformation or permanent damage such as microcracking to the circuit board. With increasing circuit densities, the amount of tolerable deformation is significantly decreased and the amount of circuit boards which pass quality standards is also reduced. Hence, the differential thermal strains dictate the reliability of the package.

The ability to design more dimensionally stable boards depends on accurate determination of the thermomechanical properties. The in-plane and out-of-plane coefficients of thermal expansion (CTE) of the woven glass/epoxy substrate are particularly important. During many of the soldering processes, the temperature exceeds the glass transition of the epoxy resin. When an epoxy is heated above the glass transition temperature (T_g), the CTE increases nearly three times its room temperature value and the elastic modulus drops by an order of magnitude. Thus, the determination of the substrate CTE above T_g is also important.

Because experimental characterization of laminates is time and labor intensive, an analytical model to predict properties of the woven substrates is desirable. Many models for predicting the properties of woven composites have been reported in the literature, several of which are summarized in a subsequent section. However, very few of these models are adapted for the two dimensional, low volume fraction geometry of the fabrics used in circuit board applications. This paper presents a combined experimental and theoretical investigation of the influence of fabric geometry (bundle size, crimp, etc.) on the properties of woven glass/epoxy substrates for multilayer circuit boards. The elastic moduli and Poisson's ratios of the boards are obtained from uniaxial tensile tests, while the CTEs of the boards are measured using thermal mechanical analysis (TMA) at temperatures above and below the glass transition. Two new models (Ockers and Sottos, 1994) are utilized for predicting the elastic properties and coefficients of thermal expansion for plain weave composites. Model predictions are compared with experimental data as well as with previous models in the literature.

Contributed by the Electrical and Electronic Packaging Division for publication in the JOURNAL OF ELECTRONIC PACKAGING. Manuscript received by the EEPD September 1, 1995; revision received September 28, 1998. Associate Technical Editor: A. Dasgupta.

Substrate Characterization

Plain Weave Geometry. The glass/epoxy substrates in most printed wire boards are fabricated using a plain weave fabric. A plain weave is composed of two sets of orthogonal fiber bundles called the warp and fill. A schematic of a unit cell for the plain weave is shown in Fig. 1. Because the thermomechanical properties of the substrate are a function of the different properties of the glass fiber bundles and epoxy resin, the geometry of the woven glass fiber bundles can have a significant effect on the overall value. For the current investigation, the fabric geometry of two commercially pressed boards (fabricated by Polyclad Inc.) was carefully characterized and related to CTE. The properties of the constituent fibers and the epoxy matrix are listed in Table 1.

The boards consisted of two layers of 2116 or 2313 fabric sandwiched between one heavy 2 oz. sheet of copper and one 1 oz. sheet of copper. Five 3.8 mm sections were cut from each laminate along a diagonal line from the center to one of the corners. The sections were cut in half and mounted so that either the warp or fill direction was exposed. The samples were then polished and carefully examined under an optical microscope for resin rich regions and variations in the microstructure which might influence dimensional stability of the laminate. Photomicrographs taken in the warp and fill directions are shown in Figs. 2 and 3 for both laminates.

The warp and fill bundles in Figs. 2 and 3 have different sizes, crimp, and volume fractions which are described by a^k, b^k, d^k, and v_f^k (see Fig. 1), where $k = w$ or f for the warp and fill directions. The aspect ratio of the bundles $(a/b)^k$ and the crimp $(h/d)^k$ were carefully measured and the results listed in

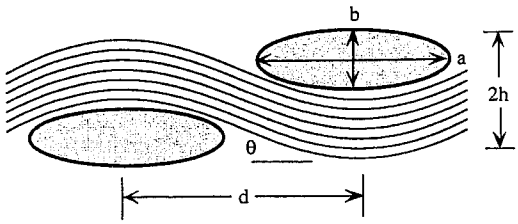

Fig. 1 Schematic of plain weave geometry

Table 2. Each value in Table 2 represents the average of at least two separate measurements from the five different locations. For both of the laminates examined, the aspect ratio and the crimp of the fill fiber bundles was larger than measured for the warp bundles. No consistent variations in bundle size or crimp were observed at the varying locations across the board. Individual volume fractions of the warp and fill yarns were measured using image analysis (orthogonal to the cross section) and are also listed in Table 2.

Determination of Elastic Modulus and Poisson's Ratio. Uniaxial tension tests were performed to determine the moduli and Poisson's ratio of two ply laminates of the 2116 and 2313 fabrics. Samples were prepared from the same commercially pressed boards described above. The copper layers on the top and bottom of the laminates were removed using a dilute nitric acid bath. Tension samples with a gage length of 30.5 cm and a width of 2.54 cm were then cut from the boards. Measured values of the Young's moduli, E_x and E_y in the warp and fill directions respectively, and the major Poisson's ratio, ν_{xy}, are listed in Tables 3 and 4 for the two different laminates. The value of the elastic modulus in the warp direction is higher than in the fill direction for both laminates due to the lower bundle crimp in the warp direction. The effect is more pronounced for the 2313/2313 laminate which has a larger variation in crimp between warp and fill.

Thermal Expansion Measurements. The in-plane CTEs of the two commercially pressed boards were measured using thermal mechanical analysis (TMA) at temperatures above and below the glass transition. Rectangular samples approximately 0.5 cm × 2.0 cm were cut from the boards (with copper removed) and mounted in a special thin film fixture to accommodate the small sample thickness. The temperature was increased from −20°C to 180°C at a rate of 5°C/min.

A typical TMA scan showing both the dimensional change and the calculated CTE is shown in Fig. 4. The expansion is linear and the CTE nearly constant below the glass transition. At 100°C the expansion becomes nonlinear and the CTE increases rapidly reaching a maximum at about 125°C. After this peak, the expansion drops quickly to a value lower than at room temperature. Although there is considerable scatter in the data above T_g, the value at 175°C is reported.

Average experimental CTE values are listed in Tables 5 and 6 at a temperature less than T_g (25°C) and greater than T_g (175°C). The value of the in-plane CTEs in the warp direction are lower than in the fill direction below T_g for both laminates again due to the lower bundle crimp in the warp direction.

Table 1 Properties of glass fibers and epoxy matrix

	Glass Fiber	Epoxy Matrix	
		$T<T_g$	$T>T_g$
E (GPa)	72.3	3.44	0.07
α (10^{-4}/°C)	0.051	0.58	1.97
ν	0.22	0.33	0.33
ρ (g/cm^3)	2.59	1.4	-

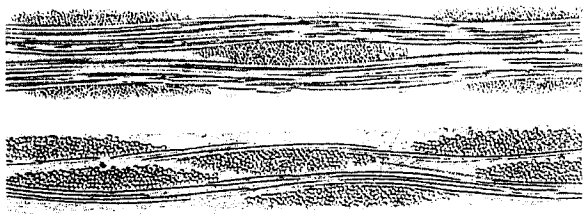

Fig. 2 Photomicrograph of 2313/2313 laminate (100×): (*a*) warp yarns parallel to the page, fill yarns perpendicular; (*b*) fill yarns parallel to the page, warp yarns perpendicular

Model Formulation

A large number of micromechanical models for predicting woven composite properties have been reported in the literature. The early models for predicting mechanical behavior used classical lamination theory (CLT) to determine the properties of an idealized unit cell which represented the warp and fill geometry. Halpin, Jerine, and Whitney (1971) proposed that a unidirectional crossply laminate with the same volume fractions in the warp and fill directions as the woven ply serves as an upper bound on the elastic properties of the woven ply. This laminate analogy of the woven ply used CLT to determine the properties of a balanced laminate consisting of two warp plies and two fill plies with properties rotated by an angle equal to the crimp angle. Ishikawa and Chou (1982a, 1982b, 1983a, 1983b) formulated two one-dimensional models for predicting the elastic properties of a woven ply. The first model, the mosaic model, views the fabric as an assemblage of two ply crossply laminates, ignoring the continuity and undulation of the fiber bundles. The properties are integrated along the length of the unit cell. Averaging the compliances (iso-stress) yields the lower bound, while averaging the stiffnesses (iso-strain) yields an upper bound. The mosaic model upper bound for a plain weave composite is the same as a unidirectional cross-ply, described by Halpin et al. (1971). The second model introduced by Ishikawa and Chou (1982a, 1982b, 1983a, 1983b), the crimp model, uses CLT to determine the properties of a thin slice in the unit cell and integrates the properties along the length of the unit cell.

A later model introduced in the work by Naik and Shembekar (1992a, 1992b, 1993) and Shembekar and Naik (1992, 1993) is based on the crimp model. This model allows for gaps between the fiber bundles, in-plane misalignments between the plies, and the two-dimensional nature in a plain weave laminate. Naik and Ganesh (1993) extended the method to predict the thermal expansion coefficients. Another model by Pandey and Hahn (1992) used an iso-strain assumption along with geometric efficiency factors to predict the elastic moduli and expansion coefficients. Lien et al. (1984) used an idealized curved cross ply model to predict the mechanical and thermal properties of fabric reinforced printed wiring boards. In a recent work, Wu,

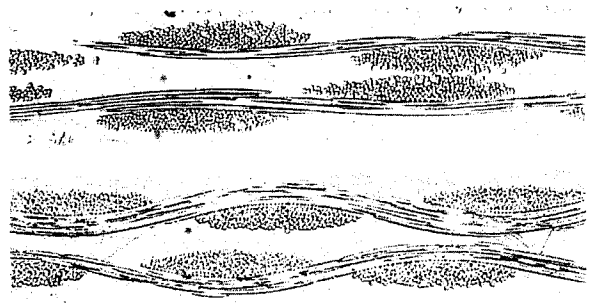

Fig. 3 Photomicrograph of 2116/2116 laminate (100×): (*a*) warp yarns parallel to the page, fill yarns perpendicular; (*b*) fill yarns parallel to the page, warp yarns perpendicular

Table 2 Measurements of bundle size and crimp

	Aspect Ratio (a/b)		Crimp (h/d)		Volume Fraction V_f	
	fill	warp	fill	warp	fill	warp
2313	7.9	5.5	0.17	0.10	31.0	40.1
2116	5.7	4.7	0.18	0.15	28.3	30.2

Guo, and Chen (1993) developed a semi-empirical engineering model to predict CTEs of epoxy-glass printed wiring boards measured above and below the glass transition temperature. Yuan and Falanga (1993) also experimentally characterized the CTE of FR-4 laminates and employed a semi-empirical model to predict the data.

Computational studies have also been utilized for determining the mechanical properties of woven composites. Shindo, Ueda, and Nishioka (1993) developed a two-dimensional plain strain finite element model of woven laminates including temperature dependence of the properties. Sankar and Marrey (1993) used a two-dimensional beam model of the weave architecture to determine the extensional, bending, and shear behavior. Bhandarkar et al. (1991) formulated a three-dimensional model to investigate the nonlinear properties of fabric reinforced circuit boards. Dasgupta and Bhandarkar (1994) used a homogenization technique to create a three dimensional finite-element model of the weave architecture.

The laminate characterization described in the previous section revealed significant differences between the fabric structure in the warp and fill directions of woven fabrics utilized for circuit board applications. A two-dimensional model is therefore necessary to accurately predict the thermomechanical properties of the board. This paper utilizes two simple micromechanical models for predicting thermoelastic properties of woven glass laminates. A two-dimensional "equivalent" laminate model (EQLAM) which is similar to previous models which use classical lamination theory and a unique blending model (BLEND) are developed to incorporate the fabric microstructure characterized in the commercially pressed boards. Both models are summarized below.

Equivalent Laminate Model. The "equivalent" laminate model (EQLAM), shown schematically in Fig. 5, idealizes the woven fabric laminate as a symmetric three-ply crossply laminate. The fibers in the warp and fill directions of the unit cell are separated and represented as three individual plies. The plies are arranged as a symmetric crossply laminate with a fill ply in the center of thickness b^f sandwiched between two warp plies of thickness $b^w/2$ each, such that the total thickness, $t = (b^w + b^f)$. Micromechanical relationships developed using a composite cylinder assemblage (also known as self consistent field) model are first used to calculate the transversely isotropic properties of the warp and fill plies as if the fiber bundles had zero crimp. Details of the self consistent composite cylinder model are given in Whitney and McCullough (1990). The compliance components of these plies are represented by s_{11}^k, s_{12}^k, s_{22}^k, s_{23}^k, s_{44}^k, s_{55}^k, s_{66}^k, and the in-plane CTEs denoted by α_1^k, α_2^k, where $k = w$ or f for the warp or fill directions, respectively. Using the weave geometry in Table 2 to describe the undulation of the ply, coordinate transformations are used to find the properties $s_{ij}'^k(x)$ and $\alpha_i'^k(x)$ of a small portion dx of the ply at a position x in terms of the compliance and CTEs of the unidirectional ply. The equivalent orthotropic properties of the warp and fill ply are found by integrating the rotated properties along the length of the ply as follows:

$$\bar{s}_{ij}^k = \frac{1}{2d}\int_0^{2d} s_{ij}'^k(x)dx \tag{1}$$

$$\bar{\alpha}_i^k = \frac{1}{2d}\int_0^{2d} \alpha_i'^k(x)dx, \tag{2}$$

where the length d is as shown in Fig. 1. Details of the calculations are outlined in the appendix.

CLT is then applied to the entire equivalent laminate of the unit cell, whereas previous undulation models (Ishikawa and Chou, 1982a, 1982b, 1983a, 1983b) apply CLT to every infinitesimal segment along the length of the plain weave unit cell. The compliance matrix is inverted to yield the components of the ply stiffness matrix, Q_{ij}^k, which are then used to calculate the laminate extensional stiffness matrix $[A]$. In CLT, the components, A_{ij}, are expressed as

$$A_{ij} = b^w Q_{ij}^w + b^f Q_{ij}^f, \tag{3}$$

and the warp and fill ply stiffness are given by

$$Q_{11}^k = \frac{E_1^k}{1 - \nu_{12}^k \nu_{21}^k} \quad Q_{12}^k = \nu_{12}^k Q_{22}^k$$

$$Q_{22}^k = \frac{E_2^k}{1 - \nu_{12}^k \nu_{21}^k} \quad Q_{66}^k = G_{12}^k. \tag{4}$$

The elastic properties of the laminate are calculated from the well known expressions

$$E_x = \frac{A_{11}A_{22} - A_{12}^2}{A_{22}t} \quad G_{xy} = \frac{A_{66}}{t}$$

$$E_y = \frac{A_{11}A_{22} - A_{12}^2}{A_{11}t} \quad \nu_{xy} = \frac{-A_{12}}{A_{22}}. \tag{5}$$

The CTEs of the laminate are then determined from the following:

Table 3 Mechanical properties of 2313/2313 laminate

	E_x (GPa) *warp*	E_y (GPa) *fill*	ν_{xy}
Experiment	20.8 ± .3	14.1 ± .5	.131 ± .04
EQLAM-I	21.9	15.6	0.238
BLEND	20.8	14.0	0.155
EQLAM-II	20.3	14.3	0.260

Table 4 Mechanical properties of 2116/2116 laminate

	E_x (GPa) *warp*	E_y (GPa) *fill*	ν_{xy}
Experiment	17.7 ± .3	16.2 ± .2	.110 ± .02
EQLAM-I	17.7	17.2	0.207
BLEND	16.5	15.0	0.136
EQLAM-II	15.8	15.1	0.236

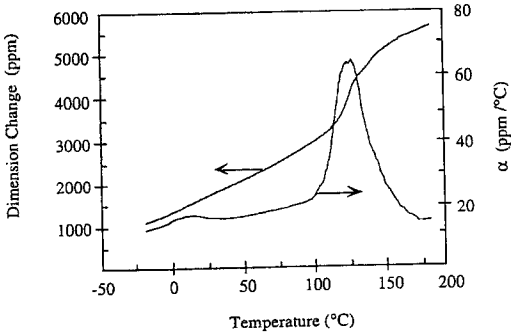

Fig. 4 Expansion measured by thermal mechanical analysis (TMA) and calculated CTE for the 2313/2313 laminate in the warp direction

Table 5 In-plane CTEs of 2313/2313 laminate

	α_x (10^{-4}/°C) warp		α_y (10^{-4}/°C) fill	
	T<Tg	T>Tg	T<Tg	T>Tg
Experiment	0.150	0.08	0.192	0.16
EQLAM-I	0.165	0.09	0.251	.126
BLEND	0.145	0.06	0.199	.131

$$\alpha_x = \frac{A_{22}(b^w\chi_1 + b^f\chi_2) - A_{12}(b^w\chi_3 + b^f\chi_4)}{A_{11}A_{22} - A_{12}^2}$$

$$\alpha_y = \frac{A_{11}(b^w\chi_1 + b^f\chi_2) - A_{12}(b^w\chi_3 + b^f\chi_4)}{A_{11}A_{22} - A_{12}^2}, \quad (6, 7)$$

where

$$\chi_1 = Q_{11}^w\alpha_1^w + Q_{12}^w\alpha_2^w$$
$$\chi_2 = Q_{11}^f\alpha_1^f + Q_{12}^f\alpha_2^f$$
$$\chi_3 = Q_{12}^w\alpha_1^w + Q_{22}^w\alpha_2^w$$
$$\chi_4 = Q_{12}^f\alpha_1^f + Q_{22}^f\alpha_2^f. \quad (8)$$

In the formulation described above, compliances were averaged and used to calculate an equivalent compliance matrix for each ply according to Eq. (1). An alternate formulation can also be used such that the stiffness components, $c_{ij}'^k(x)$ are averaged, and an equivalent stiffness matrix calculated for each ply in a similar fashion:

$$\bar{c}_{ij}^k = \frac{1}{2d}\int_0^{2d} c_{ij}'^k(x)dx. \quad (9)$$

Averaging the compliances using Eq. (1) will lead to a lower bound on the elastic moduli, while averaging the stiffnesses using Eq. (9) will lead to an upper bound.

Blending Model. The basic strategy of the blending model (BLEND), shown schematically in Fig. 6 is to first calculate the properties of an "intermediate" matrix using the geometry and properties of the fill bundles. First, the compliance s_{ij}^f and CTE α_i^f of the fill ply are calculated from the properties of the fiber and matrix assuming the bundles are straight. Then, using the geometry of the fill bundles, the properties $\alpha_i'^f(x)$ and $s_{ij}'^f(x)$ of a small section dx of the fiber is found from a rotation about the y-axis. The compliance matrix and CTEs are then integrated along the length of the fiber using Eqs. (1) and (2), yielding an orthotropic fill ply with properties denoted by $\bar{s}_{ij}^f$ and $\bar{\alpha}_i^f$. Hence, the fill yarns are homogenized to produce a continuum in which the warp yarns are embedded. The properties of the warp bundles are rotated and averaged in a similar manner and denoted by $\bar{s}_{ij}^{wb}$ and $\bar{\alpha}_i^{wb}$. Rather than using classical lamination theory, micromechanical relationships are employed to combine the orthotropic fill ply with the orthotropic warp bundles. Longitudinal properties are calculated with simple rule of mixtures relations, while the transverse properties are calculated with the Halpin-Tsai equation. The ξ parameter in the Halpin-Tsai equation is determined using a mechanics of materials combination rule which incorporates the influence of bundle geometry and volume fraction in the calculation of transverse properties such that (Whitney and McCullough, 1990):

$$\xi = \frac{v_{mp}v_f^w}{1 - v_{mp} - v_f^w}; \quad v_{mp} = \frac{b^f}{b^f + b^w}. \quad (10)$$

Property Predictions

Elastic Modulus and Poisson's Ratio. Predictions for elastic moduli and Poisson's ratio were made using both the equivalent laminate model (EQLAM) and the blending model (BLEND) described in the previous section. The calculations utilized the geometric properties in Table 2 and the individual glass fiber and epoxy matrix properties listed in Table 1. Model predictions are tabulated in Tables 3 and 4 and compared with experimental measurements for E_x, E_y, and ν_{xy}. For the equivalent laminate formulation, property values calculated by averaging compliances using Eq. (1) are denoted by EQLAM-II in Tables 3 and 4, while values calculated by averaging stiffnesses using Eq. (9) are denoted by EQLAM-I. The two EQLAM

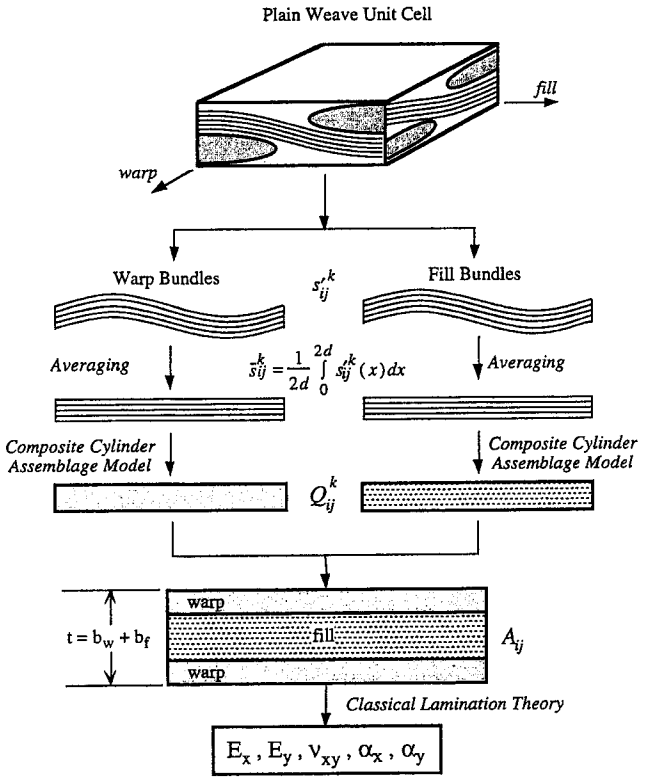

Fig. 5 Schematic of the equivalent laminate model (EQLAM)

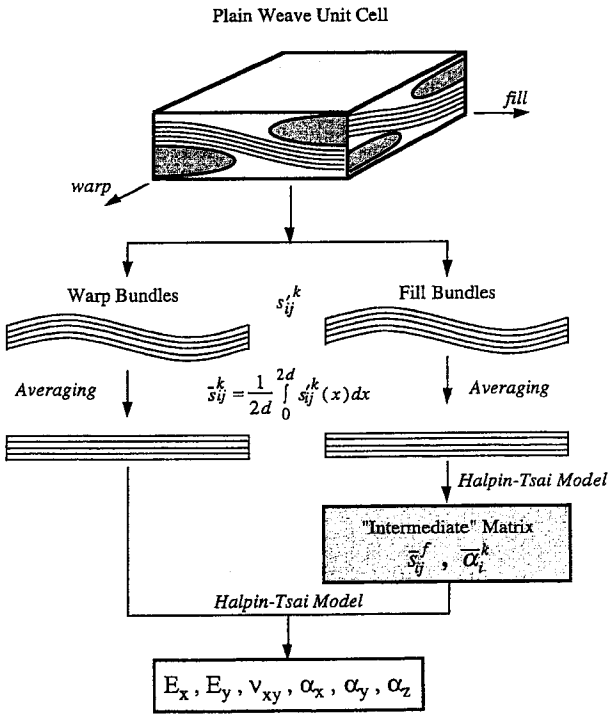

Fig. 6 Schematic of the blending model (BLEND)

Table 6 In-plane CTEs of 2116/2116 laminate

	α_x (10^{-4}/°C) warp		α_y (10^{-4}/°C) fill	
	$T<T_g$	$T>T_g$	$T<T_g$	$T>T_g$
Experiment	0.180	0.14	0.185	0.12
EQLAM-I	0.212	0.12	0.220	0.13
BLEND	0.184	0.07	0.181	0.15

predictions provide an upper and lower bound on the experimental modulus values within experimental error. The BLEND model, however, more accurately predicts the elastic modulus within these bounds. For Poisson's ratio, the BLEND model prediction is much closer to the experimental value than either of the equivalent laminate model predictions. The equivalent laminate model, like many previous models, utilizes classical lamination theory (CLT) for the prediction of the thermoelastic properties while the blending model does not. Many of the assumptions inherent to CLT such as no transverse shear cause the EQLAM formulations to significantly over predict the Poisson's ratio.

In-Plane CTEs. The in-plane CTEs for both the 2116 and 2313 laminates were also predicted using the equivalent laminate and blending models described above. Again, the calculations utilized the geometric properties in Table 2 and the individual glass fiber and epoxy matrix properties listed in Table 1. CTE predictions are tabulated in Tables 5 and 6 and compared with TMA measurements both above and below the T_g. The blending model (BLEND) predicts the experimental data below T_g more accurately than the equivalent laminate model (EQLAM-I) for both laminates. Like for Poisson's ratio, the CLT based equivalent laminate model significantly over estimates the CTE values. Note that the EQLAM-II formulation is not included in Tables 5 and 6 because it leads to even higher predictions.

Because both the equivalent laminate and blending models are based on linear elastic material behavior, neither is truly valid for predicting properties above the glass transition. Additionally, the scatter in the experimental data above T_g is considerable making it difficult to assess the accuracy of the models in this range. For the calculations of CTE above T_g, the resin Poisson's ratio was assumed to remain constant ($\nu_m = 0.33$). Although the Poisson's ratio may actually approach a value of 0.5 above T_g, the exact value is not well defined. The analysis by Wu, Guo, and Chen (1993) makes a similar assumption. Fortunately, parametric studies with the model have shown that changes in Poisson's ratio have only a small effect on the CTE values calculated in Tables 5 and 6. Both models predict lower CTE values above T_g, which is representative of the experimental data. The decrease in CTE is due to the dominance of fiber properties as the resin drops in stiffness above the glass transition.

Out-of-Plane CTEs. Predictions of the out-of-plane CTE, α_z, for both the 2313 and 2116 laminates are listed in Table 7. Values were calculated using only the BLEND model because the classical lamination assumptions involved in the EQLAM model give poor approximations of the properties in the thickness direction of the laminate. The out-of-plane CTEs are dominated by the resin properties and are significantly higher than the in-plane values. A dramatic increase in value is predicted above T_g, which corresponds with the increase in resin CTE. Unfortunately, accurate experimental measurements of α_z to compare with the BLEND predictions could not be made with the TMA apparatus used for the in-plane measurements.

Table 7 BLEND predictions of out-of-plane CTEs

	α_z (10^{-4}/°C)	
	$T<T_g$	$T>T_g$
2313/2313	.515	1.72
2116/2116	.527	1.77

Comparison With Other Models

Property predictions were compared with several other models in the literature. To facilitate comparison, only a single ply 2116 fabric composite was considered. The thermoelastic properties calculated using the constituent properties in Table 1 and the bundle size and crimp in Tables 2 are listed in Table 8. The properties of the single ply composite are slightly different than for the two ply composite reported in Table 4 because nesting of fiber bundles in a processed two ply laminate leads to slightly higher volume fractions than if the plies were considered separately.

The mosaic model (Ishikowa and Chou, 1982, 1983) serves as an upper bound for the prediction of elastic moduli. The EQLAM model provides a tighter upper and lower bound on the moduli. The moduli predictions of the EQLAM and BLEND models seem to be consistent with the mosaic model, while the crimp (Ishikowa and Chou, 1982, 1983) model predicts significantly lower values. The predictions of the blending model for Poisson's ratio and in-plane coefficients of thermal expansion are consistently lower than the remainder of the models.

Parametric Studies

Parametric studies were performed using the blending model to assess the influence of yarn crimp on the elastic modulus and CTEs of the woven plies. The variation of E_x, α_x, and α_z with warp bundle crimp is plotted in Fig. 7. In all of these plots, the property values have been normalized by dividing by the value for the case of zero crimp. Hence, for $h/d = 0$, the modulus and CTEs are the same as the longitudinal modulus and CTEs of a unidirectional cross ply laminate of similar volume fraction. Also, due of the two-dimensional nature of the physical weave constraints, the increase in crimp in the warp direction causes a corresponding decrease in crimp in the fill direction.

At very small values of h/d the change in properties is minimal. As the crimp increases further, E_x starts to decrease rapidly, while α_x increases. At higher values of crimp, the properties in the warp direction approach the transverse properties of a unidirectional ply of the same volume fraction. The out-of-plane CTE, α_z, decreases steadily as the crimp increases due to rotation of the lower CTE fibers in the z-direction.

Conclusions

The fabric geometry of two commercially pressed circuit boards was characterized using optical microscopy. Significant differences in bundle size, crimp and volume fraction were measured in the warp and fill directions. These changes in fabric geometry were found to have a significant effect on the thermomechanical properties of the woven composite. Lower crimp and higher fiber volume fraction led to lower in-plane CTEs and higher modulus.

Table 8 Properties of a single 2116 ply

	E_x (GPa)	E_y (GPa)	ν_{xy}	α_x (10^{-4}/°C)	α_y (10^{-4}/°C)	α_z (10^{-4}/°C)
MOSAIC	16.5	16.2	0.208	0.283	0.284	0.528
EQLAM-I	15.9	15.6	0.216	0.229	0.238	0.307
BLEND	15.0	13.5	0.139	0.199	0.198	0.551
CRIMP	12.9	8.69	0.270	—	—	—
EQLAM-II	14.3	13.7	0.244	0.238	0.250	0.307

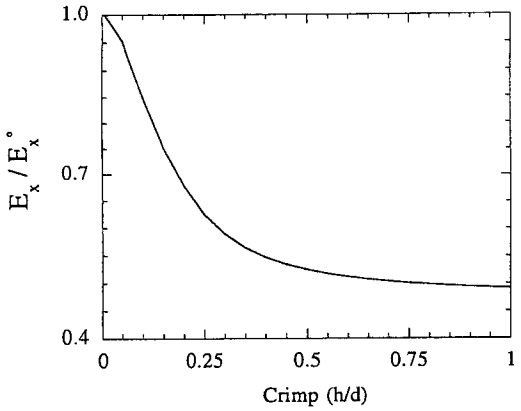

Fig. 7(*a*) Predicted variation of E_x with fabric crimp

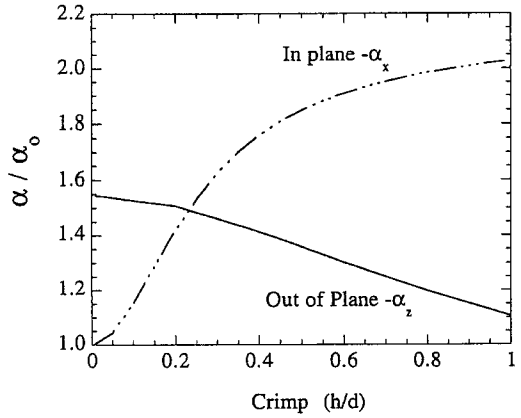

Fig. 7(*b*) Predicted variation of α_x and α_z ($T < T_g$) with fabric crimp

Two new models for predicting the properties of plain weave composites were formulated. Predictions of these models were compared with previous models in the literature as well as experimental data. All models yielded fairly consistent predictions of the in-plane elastic moduli. However, models such as the equivalent laminate model (EQLAM) which utilize CLT over predicted the values of ν_{xy}, α_x, and α_y. The assumption of no transverse shear inherent in CLT leads to the inaccurate predictions of these properties. Use of higher order lamination theory may improve accuracy in these models. The results of the blending model (BLEND), which did not use CLT, resulted in improved predictions of ν_{xy}, α_x, and α_y when compared with experiments.

Acknowledgments

The authors gratefully acknowledge the financial support of Owens Corning Fiberglas, technical assistance from Doug Lyle and Robert Sauer at Owens Corning, and the donation of material by Polyclad, Inc.

References

Bhandarkar, S., Dasgupta, A., Pecht, M., and Barker, D., 1991, "Non-Linear Thermo-Mechanical Properties of Fabric Reinforced Printed Wiring Boards," Proceedings, 5th International SAMPE Electronics Conference, June 18–20, Society for the Advancement of Material and Process Engineering, Covina, CA, pp. 248–257.

Dasgupta, A., and Bhandarkar, S. M., 1994, "Effective Thermomechanical Behavior of Plain-Weave Fabric-Reinforced Composites Using Homogenization Theory," *Journal of Engineering Materials and Technology,* Vol. 116, No. 1, pp. 99–105.

Halpin, J. C., Jerine, K., and Whitney, J. M., 1971, "The Laminate Analogy for 2 and 3 Dimensional Composite Materials," *J. of Composite Materials,* Vol. 5, pp. 36–49.

Ishikawa, T., and Chou, T.-W., 1982a, "Elastic Behavior of Woven Hybrid Composites," *Journal of Composite Materials,* Vol. 16, pp. 2–19.

Ishikawa, T., and Chou, T.-W., 1982b, "Stiffness and Strength Behavior of Woven Fabric Composites," *Journal of Materials Science,* Vol. 17, pp. 3211–3220.

Ishikawa, T., and Chou, T.-W., 1983a, "One-Dimensional Micromechanical Analysis of Woven Fabric Composites," *AIAA Journal,* Vol. 21, No. 12, pp. 1714–1721.

Ishikawa, T., and Chou, T.-W., 1983b, "In-Plane Thermal Expansion and Thermal Bending Coefficients of Fabric Composites," *Journal of Composite Materials,* Vol. 17, pp. 92–104.

Lekhnitskii, S. G., 1963, *Theory of Elasticity for an Anisotropic Body,* Holden-Day, San Francisco.

Lien, S. Y., Thompson, D. G., Hemler, P. F., and Williamson, M., 1984, "Prediction of Mechanical Properties of Woven Fabric Composites," Proceedings, 16th National SAMPE Technical Conference, October 9–11, Society for the Advancement of Material and Process Engineering, Covina, CA, pp. 249–257.

Naik, N. K., and Shembekar, P. S., 1992a, "Elastic Behavior of Woven Fabric Composites: I—Lamina Analysis," *Journal of Composite Materials,* Vol. 26, No. 15, pp. 2196–2225.

Naik, N. K., and Shembekar, P. S., 1992, "Elastic Behavior of Woven Fabric Composites: III—Laminate Design," *Journal of Composite Materials,* Vol. 26, No. 17, pp. 2522–2541.

Naik, N. K., and Shembekar, P. S., 1993a, "Elastic Analysis of Woven Fabric Laminates: Part II—Mixed Composites," *Journal of Composites Technology & Research,* JCTRER, Vol. 15, No. 1, pp. 34–37.

Naik, N. K., and Ganesh, V. K., 1993b, "Prediction of Thermal Expansion Coefficients of Plain Weave Fabric Composites," *Composite Structures,* Vol. 26, pp. 139–154.

Ockers, J., and Sottos, N. R., 1994, "Thermoelastic Properties of Plain Weave Composites for Circuit Board Applications: A Comparison of Models and Experiments," Proceedings, American Society for Composites 9th Technical Conference, Sept. 20–22, Technomic, Lancaster, PA, p. 1126–1134.

Pandey, R., and Hahn, H. T., 1992, "A Micromechanics Model for 2D Fabrics," Proceedings, American Society for Composites, 7th Technical Conference, October 13–15, Technomic, Lancaster, PA, pp. 359–368.

Sankar, B. V., and Marrey, R. V., 1993, "A Unit-Cell Model of Textile Composite Beams for Predicting Stiffness Properties," *Composites Science and Technology,* Vol. 49, pp. 61–69.

Shembekar, P. S., and Naik, N. K., 1992, "Elastic Behavior of Woven Fabric Composites: II—Laminate Analysis," *Journal of Composite Materials,* Vol. 26, No. 15, pp. 2226–2246.

Shembekar, P. S., and Naik, N. K., 1993, "Elastic Analysis of Woven Fabric Laminates: Part I—Off-Axis Loading," *Journal of Composites Technology & Research,* JCTRER, Vol. 15, No. 1, pp. 23–33.

Shindo, Y., Ueda, S., and Nishioka, Y., 1993, "Mechanical Behavior of Woven Composites at Low Temperatures," *Fusion Engineering and Design,* Vol. 20, pp. 469–474.

Whitney, J. M., and McCullough, R. L., 1990, *Micromechanical Materials Modeling,* Vol. 2, Delaware Composites Design Encyclopedia, Technomic Publishing Company, Lancaster, PA.

Wu, T. Y., Guo, Y., and Chen, W. T., 1993, "Thermal-Mechanical Strain Characterization for Printed Wiring Boards," *IBM J. Res. Develop.,* Vol. 37, No. 5, pp. 621–634.

Yuan, J., and Falanga, L. A., 1993, "The In-Plane Thermal Expansion of Glass Fabric Reinforced Epoxy Laminates," *Journal of Reinforced Plastics and Composites,* Vol. 12, pp. 489–496.

APPENDIX

Both of the models presented in this paper represent undulated fiber bundles or plies with effective straight bundles or plies. The basic strategy is to calculate the average elastic properties by integrating the rotated compliances or stiffnesses along the length of undulation. A schematic of the bundle geometry is shown in Fig. A1. The fiber bundles undulate in the x-z plane following a cosine curve described by

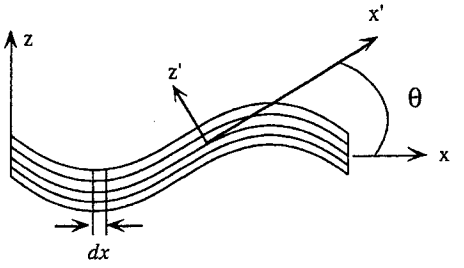

Fig. A1 Schematic of undulating fiber bundle

$$z(x) = \frac{h}{2}\cos\left(\frac{\pi}{d}x\right). \tag{A.1}$$

If the fibers are assumed straight but oriented at an angle θ over a small section dx of the bundle, the compliance (or stiffness) components are easily calculated from standard micromechanical relationships for a transversely isotropic composite when the principal axis are rotated in the x'-z' plane. The angle of rotation, θ, is given by the slope of the curve

$$\theta(x) = -\tan^{-1}\left(\frac{dz}{dx}\right). \tag{A.2}$$

The local compliance components of the fiber bundle in the x-z coordinate system, $s'_{ij}(x)$, are then found by performing coordinate transformations on the small section dx of the bundle following the procedure outlined in Lekhinitski (1963). The rotated compliances are then averaged along the length of the fiber,

$$\bar{s}_{ij} = \frac{1}{2d}\int_0^{2d} s'_{ij}(x)dx \quad (i, j = 1, 2, 6). \tag{A.3}$$

The resulting average compliances of the bundles are given by

$$\bar{s}_{11} = \frac{s_{11}\left(1+\frac{c}{2}\right) + (2s_{12}+s_{55})\left(\frac{1}{2}c\right) + s_{22}\left[(1+c)^{3/2} - \left(1+\frac{3}{2}c\right)\right]}{(1+c)^{3/2}}$$

$$\bar{s}_{12} = \frac{s_{12} + s_{23}(\sqrt{1+c}-1)}{\sqrt{1+c}}$$

$$\bar{s}_{13} = \frac{(s_{11}+s_{22}-s_{55})\left(\frac{1}{2}c\right) + s_{12}[(1+c)^{3/2}-c]}{(1+c)^{3/2}}$$

$$\bar{s}_{22} = s_{22}$$

$$\bar{s}_{23} = \frac{s_{23} + s_{12}(\sqrt{1+c}-1)}{\sqrt{1+c}}$$

$$\bar{s}_{33} = \frac{\left[(1+c)^{3/2} - \left(1+\frac{3}{2}c\right)\right] + s_{22}\left(1+\frac{c}{2}\right) + (2s_{12}+s_{55})\left(\frac{1}{2}c\right)}{(1+c)^{3/2}}$$

$$\bar{s}_{44} = \frac{s_{44} + s_{55}(\sqrt{1+c}-1)}{\sqrt{1+c}}$$

$$\bar{s}_{55} = \frac{s_{55}[(1+c)^{3/2}-c] + 2(s_{11}-4s_{12}+2s_{22}-s_{55})\left(\frac{1}{2}c\right)}{(1+c)^{3/2}}$$

$$\bar{s}_{66} = \frac{s_{55} + s_{44}(\sqrt{1+c}-1)}{\sqrt{1+c}}$$

$$c = \left(\frac{\pi h}{2d}\right)^2 \tag{A.4}$$